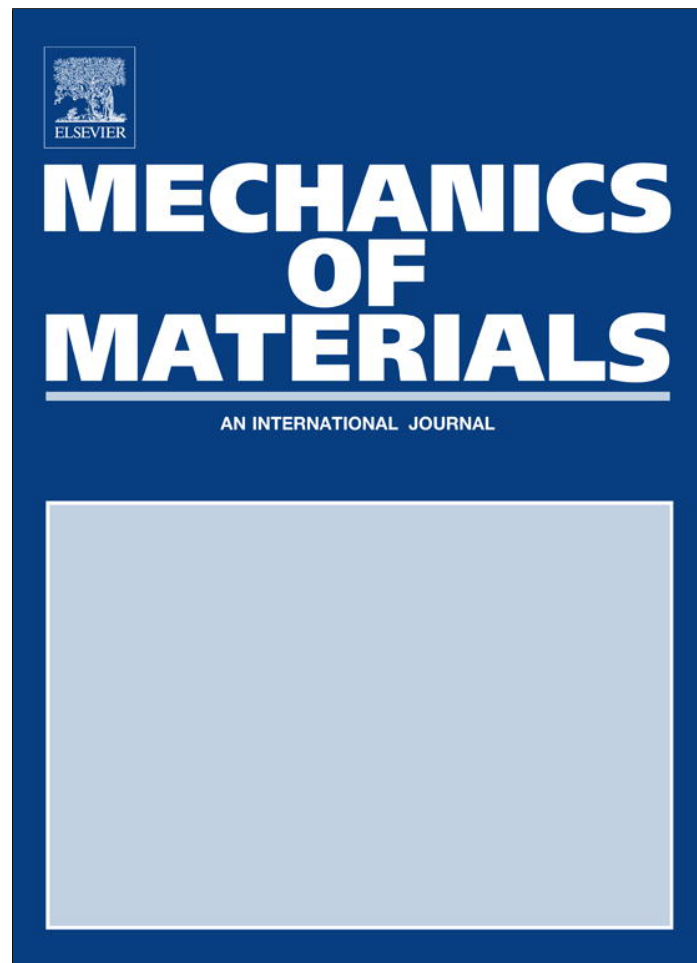


Provided for non-commercial research and education use.
Not for reproduction, distribution or commercial use.



(This is a sample cover image for this issue. The actual cover is not yet available at this time.)

This article appeared in a journal published by Elsevier. The attached copy is furnished to the author for internal non-commercial research and education use, including for instruction at the authors institution and sharing with colleagues.

Other uses, including reproduction and distribution, or selling or licensing copies, or posting to personal, institutional or third party websites are prohibited.

In most cases authors are permitted to post their version of the article (e.g. in Word or Tex form) to their personal website or institutional repository. Authors requiring further information regarding Elsevier's archiving and manuscript policies are encouraged to visit:

<http://www.elsevier.com/copyright>

Contents lists available at [SciVerse ScienceDirect](#)

Mechanics of Materials

journal homepage: www.elsevier.com/locate/mechmat

Effects of manufacturing inhomogeneities on strength properties of float glass



Gergely Molnár*, Imre Bojtár

Budapest University of Technology and Economics, Department of Structural Mechanics, Műegyetem rkp. 3. K mf. 63, 1111 Budapest, Hungary

ARTICLE INFO

Article history:

Received 13 March 2012

Received in revised form 12 September 2012

Available online 22 December 2012

Keywords:

Inhomogeneities

Micro-CT

Structural glass

Statistical simulation

Size effect

Eshelby method

ABSTRACT

This study deals with a statistically defined mechanical effect of the inhomogeneities remaining in structural glass plates after the manufacturing by floating process. Our goal was to define a stress limit that will not be exceeded with a 95% probability. We used Monte Carlo simulation to calculate the stress peaks that appear in structural glass.

First we made micro-CT images of the inhomogeneities to describe the precise geometry. Then we used analytical Eshelby solution and finite element method to calculate the stress fields around an ellipsoidal inclusion. Knowing the statistical distribution of the inhomogeneities we built a MATLAB simulation, which was used to calculate the factoring coefficient, representing statistically relevant stress peaks. With this model we were able to define a size effect coefficient allowing us to propose simple guidelines to minimise the effect of the remaining defects.

© 2012 Elsevier Ltd. All rights reserved.

1. Introduction

In float glass manufacture the appearance of inhomogeneities – such as voids or rigid inclusions, optical defects – cannot be avoided. Also the defects could dramatically reduce the quality grade of the product. Float glass is known to have micro-inhomogeneities due to its amorphous molecular structure (Benedetti et al., 1994). In the present study we focus on the mechanical effect of the mesoscopic defects. During the past decades the inspection of these mesoscopic defects was done by human-eyes. Nowadays manufacturing factories use online defect inspection systems (Peng et al., 2008; Jin et al., 2011). Using machine vision should make the quality control reliable and accurate. The 2D optical classification of the inhomogeneities is presented in Liu et al. (2011) and Peng et al. (2011). We note that these authors did not use a mechanical approach to compute the effect of the remaining defects. Therefore to use glass as a structural material confidently

we have to calculate the exact mechanical effect of the inhomogeneities.

The aim of the present study was to investigate the effect of the mesoscopic defects on the effective strength properties of the structural glass. There are only a few inhomogeneities in structural glass plate, so we can neglect the reciprocal mechanical effect. Therefore our analysis aimed to statistically define a stress limit (using numerical simulation) which will not be exceeded with 95% probability. We could use the coefficient to multiply the applied load in a design standard (effect side in Eurocode) without taking into account the strength (resistance side) of the glass. With the help of the defined indicator coefficient we would like to suggest simple design guidelines, which are capable of minimising the mechanical effect of the defects in glass.

In a previous study (Molnár et al., 2012) we examined the mesoscopic material structure of glass. We divided a glass plate into regions as the external surface, the edge and the glass volume itself. We found that originally the edge has the major stress generating factor, the largest stress peaks were found on a grinded edge, but if we polish the edge, the already existing inside inclusions could

* Corresponding author. Tel.: +36 20 290 75 66.

E-mail addresses: gmolnar@mail.bme.hu (G. Molnár), ibojtard@mail.bme.hu (I. Bojtár).

present the largest mechanical errors in the material. According to micro-CT scans we have considered the inside surface of the voids perfect, free from environmental corrosion.

To reach our goal first we needed the exact 3D geometry of the voids (bubbles) and the rigid stones. We carried out micro computed tomography (micro-CT) scans to determine the shape and the size of the defects followed by optical microscopy to collect statistical information about the density function of the radii ratio of the spheroid voids.

With the geometrical data we built finite element models, which were used to compute the stress distribution around a single inclusion in the glass in real environment. Then we used an equivalent inclusion method programed by Meng et al. (2011). After the comparison we were able to perform the statistical analysis of the inclusions.

Throughout this report we shall refer to soda-lime-silica as glass. We limited our investigation to nominally 4 mm thick glass plates.

2. Stress distribution around ellipsoidal inclusions

According to Bartuška et al. (2001) we could distinguish three types of defects, the gaseous inhomogeneities (bubbles), crystalline inclusions (stones) and glassy inhomogeneities (cords).

The ASTM (American Society for Testing and Materials) defines the cords as glassy (not crystalline) inclusion with optical properties differing from the base (surrounding) glass. These defects have the same density as the base glass, so they did not show up on the micro-CT scans at all. According to our statistical information less than 5% of the remaining defects were cords, therefore further on we are not going to deal with the glassy inhomogeneities in the present study.

Crystalline inclusions are imperfectly melted material compounds, so they had only a slightly different density than glass (Fig. 1). These inclusions have different mechanical properties (due to the different molecular structures they are not amorphous), different thermal expansion coefficient, and almost no light transmittance ability.

Bubbles could be generated by various sources, as the decomposition of raw materials, nucleation growth,

chemical, electrochemical and mechanical reactions. In the manufacturing process bubbles play a double role. Their effect is mostly favourable, because they promote the conversion of molten glass in early stages of glass melting, but the remaining bubbles represent an unacceptable, stress concentrating defect in the product. (Bartuška et al., 2001)

The micro-CT images were made by Csaba Dobó-Nagy PhD in the laboratory of Department of Oral Diagnostics on Semmelweis University. We used Skyscan 1172 micro-CT to describe the geometry of the inhomogeneities in the glass. We made CT images from six bubbles and one stone. You can see bubbles in different sizes in Fig. 2. The figure shows that these defects appear in different sizes and slightly different shapes.

The bubbles were easy to recognise (Fig. 3) because they had no X-ray attenuation value.

According to the optical and micro-CT images we could conclude that the voids in glass have a prolate spheroid shape, and the rigid stones could be approximated with an oblate spheroid. During the statistical analysis performed on the defect distribution we have shown that the micro-CT measurable inhomogeneity medium in glass contains more than 99% bubbles and less than 1% stones. Therefore in the following we will deal only with the void type inhomogeneities, with the so-called bubbles. We have neglected during the mechanical analysis that the opened bubbles very close to the surface has a different mechanical behaviour than the ones inside.

The bubble's larger radius was always parallel with the drawing direction; and according to the micro-CT scans we found that it is also parallel with the glass surface. This phenomenon could be explained by the manufacturing procedure. At the temperature of 1600 °C glass melt, the bubbles have a perfect sphere shape (Bartuška et al., 2001), by cooling and drawing the melt into plane, these voids are getting also stretched in one direction. By decreasing the viscosity of the glass melt the bubbles could not form back into their original stable form. When the glass is finally solid, the inhomogeneities have a prolate spheroid shape with the larger radius parallel to the drawing direction.

First we would like to present an *analytical method*, which could be used to determine the stress field around

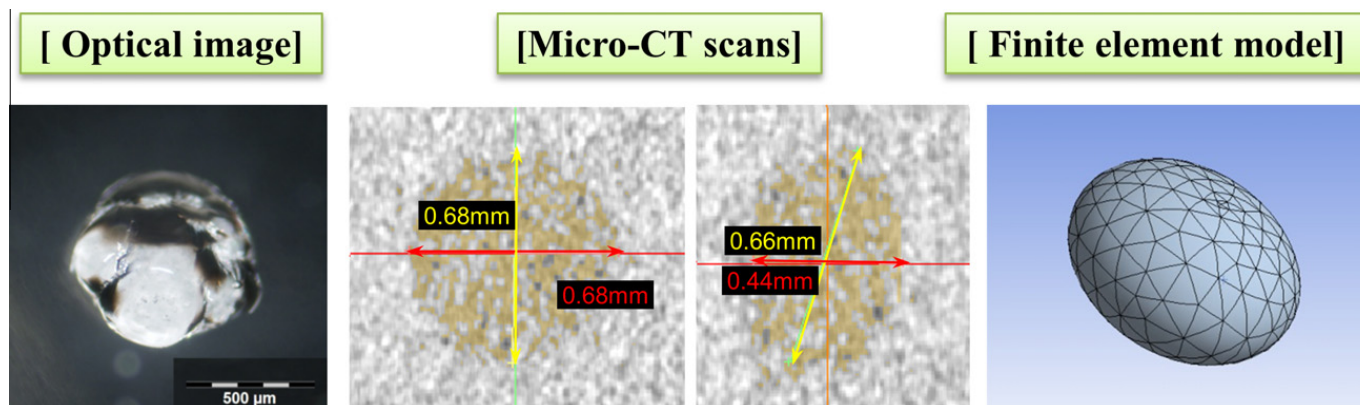


Fig. 1. FEM geometry of a batch using μ CT (Molnár et al., 2012).



Fig. 2. Bubbles in glass (optical images) (Molnár et al., 2012).

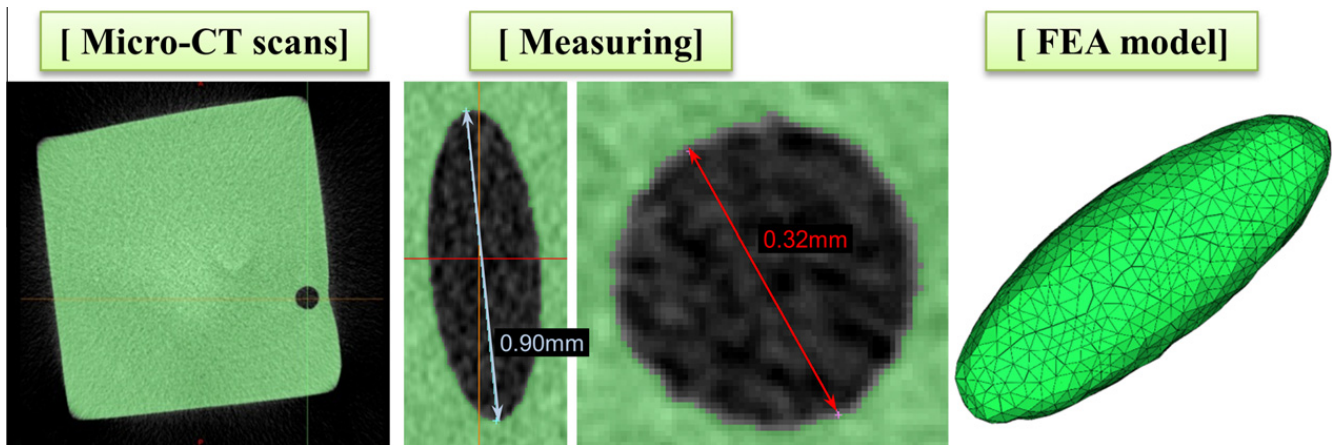


Fig. 3. Building FEM geometry of a bubble using μ CT (Molnár et al., 2012).

an ellipsoidal inhomogeneity based on Eshelby's original solution (Eshelby, 1957). We have compared the analytical results with a *finite element model* to determine that the infinite space – used for analytic solution – has any effect on the stress distribution in the real structural element. In addition, we wanted to decide which method is more accurate and which one needs less computational time. The comparison will be presented later on.

2.1. Eshelby based equivalent inclusion method

In the numerical strength analysis of glass it is important to take into account the mechanical effects of voids originated from different manufacturing process. In our calculations we applied the well-known Eshelby solution (Eshelby 1957, 1959, 1961) to determine the stress and strain concentrations around these inhomogeneities.

In the following section we would like to summarise the idea of the solution, the main theoretical steps could be found in Appendix.

The original Eshelby (Eshelby, 1957) solution was solved on a homogeneous material with an initial stress state (so-called inclusion problem). But in our case we have a void (an inhomogeneous subdomain) in a homogeneous glass matrix (D). Therefore we have to use a so-called equivalent inclusion method.

To calculate the effect of the inhomogeneity we will define an equalling arbitrary eigenstrain, which could be used in the original Eshelby's solution to describe the stress field caused by the inhomogeneity.

First we have to calculate the fictional eigenstrain, which describes the effect of the inhomogeneity. We will start with the initial condition, that in the inclusion (subdomain Ω) the stress has to be equal in the original problem and in the fictional, Eshelby's problem.

To calculate the strain and the stress peak values, we could use the following equations:

$$\begin{aligned} \hat{\varepsilon}_{ij} &= \varepsilon_{ij}^{\infty} + S_{ijkl} \varepsilon_{kl}^{**}, \\ \hat{\sigma}_{ij} &= \sigma_{ij}^{\infty} + C_{ijkl} (S_{klmn} \varepsilon_{mn}^{**} - \varepsilon_{kl}^{**}) \quad \text{in } \Omega, \\ \hat{\varepsilon}_{ij}(x) &= \varepsilon_{ij}^{\infty} + D_{ijkl}(x) \varepsilon_{kl}^{**}, \\ \hat{\sigma}_{ij}(x) &= \sigma_{ij}^{\infty} + C_{ijkl} D_{klmn}(x) \varepsilon_{mn}^{**} \quad \text{for } x \in D - \Omega. \end{aligned}$$

where $\hat{\varepsilon}_{ij}$ and $\hat{\sigma}_{ij}$ are the calculated strain and stress values, S_{ijkl} is the Eshelby's tensor, $\varepsilon_{ij}^{\infty}$ and σ_{ij}^{∞} are the strain and stress in the infinity, ε_{kl}^{**} is the initial eigenstrains, C_{ijkl} is the elastic moduli of the matrix, D_{ijkl} is a modifier matrix for the exterior points. More details could be found in Appendix.

We will use a MATLAB program made by Meng et al. (2011) to calculate the stress field around the inhomogeneity.

In the following section we would like to prove that the analytical solution which uses an infinite space could be used for the present problem. We were searching for analytical methods, because they have much less computational time than numerical ones, but for verification porpoises we used finite element results.

2.2. Numerical model

We built a small (5 × 5 × 4 mm) size cube and placed the inhomogeneity according to the micro-CT image (Fig. 4). We have modelled the precise effect of the void in a glass plate, but we reduced the number of finite elements.

We used uniform stress boundaries: unidirectional tensions – perpendicular (*x* direction) and parallel (*y* direction) to the spheroid) – and *xy* direction shear. So we could reconstruct a point's stress state of a Kirchhoff-Love plate in a smaller, mesoscopic model.

Let us consider a medium size air inclusion – a spheroidal void in the glass – with a 2:1 radii ratio. In Fig. 5 we could see that a small bubble in the material could cause a serious problem if the tension is perpendicular to the principal major axis (*y*) of the spheroid.

In every case the largest stress peak appeared in the furthest point in the perpendicular direction to the unidirectional tension.

The maximal tension stress value was independent from the spheroid's size, only the ration between the larger and the smaller radii had effect on the peak's size. We did a parametric study aimed on the maximal stress value around the prolate spheroid Fig. 6 we can see that according to the numerical tests, the stress peak could be approximated very well with a hyperbolic function.

During the *xy* directional shear test, as a result, we found that there were only τ_{xy} , and no other stress components appeared. The maximal shear peak was in Point 3 in every case. In Point 1 and 2 directly next to the void, no shear stress appeared. (Fig. 7)

Based on the numerical tests, we could state that the inhomogeneities generate a great stress peak in the glass, so we need to define the effect of these errors on the macroscopic mechanical behaviour of a structural glass plate. Therefore we need the statistical distribution of these

inhomogeneities. With the information about the position, and the quantity we could perform defect analysis using statistical methods.

With the analysis we are able to determine the mechanical effect of the inclusions in structural glass. We will be able to describe a size effect coefficient which refers to the errors not on the surface but in the glass inner structure. It is relevant because structural glass is used in tempered form, so a special tension stress distribution appears inside the glasse's volume.

With the calculated data we can prevent premature failure and the production process could be improved.

But the numerical models are time and resource consuming methods. So if we want to do a statistical calculation, we need a fast, time-effective analytical solution for the analysis.

In the next section we would like to introduce an Eshelby based equivalent inclusion method, which is capable of defining the stress distribution around an ellipsoidal inhomogeneity in an infinite space.

After these introductions we will compare the numerical and analytical solutions, to decide if we can use the Eshelby-method in our case or not.

2.3. Comparison between numerical and analytical solutions

The aim of the analysis is to calculate the stress rising effect of an ellipsoidal inhomogeneity. To compare the two methods we used a spheroid with an $a_1 = 1$ mm, and an $a_2 = a_3 = 0.5$ mm radii. We could divide the comparison into three major sections like the three simple stress state:

- unidirectional tension perpendicular (σ_x) or,
- parallel (σ_y) to the spheroid's larger axis,
- and shear stress (τ_{xy}) in the *xy* plane.

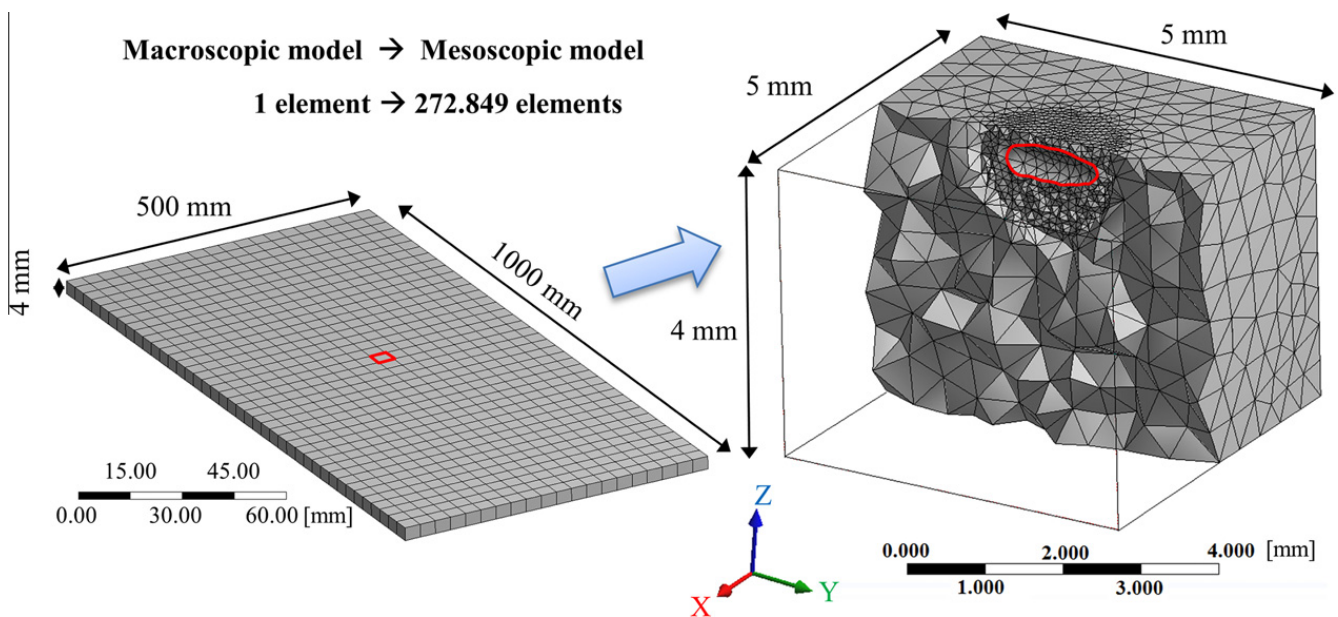


Fig. 4. Finite element model built on inclusions.

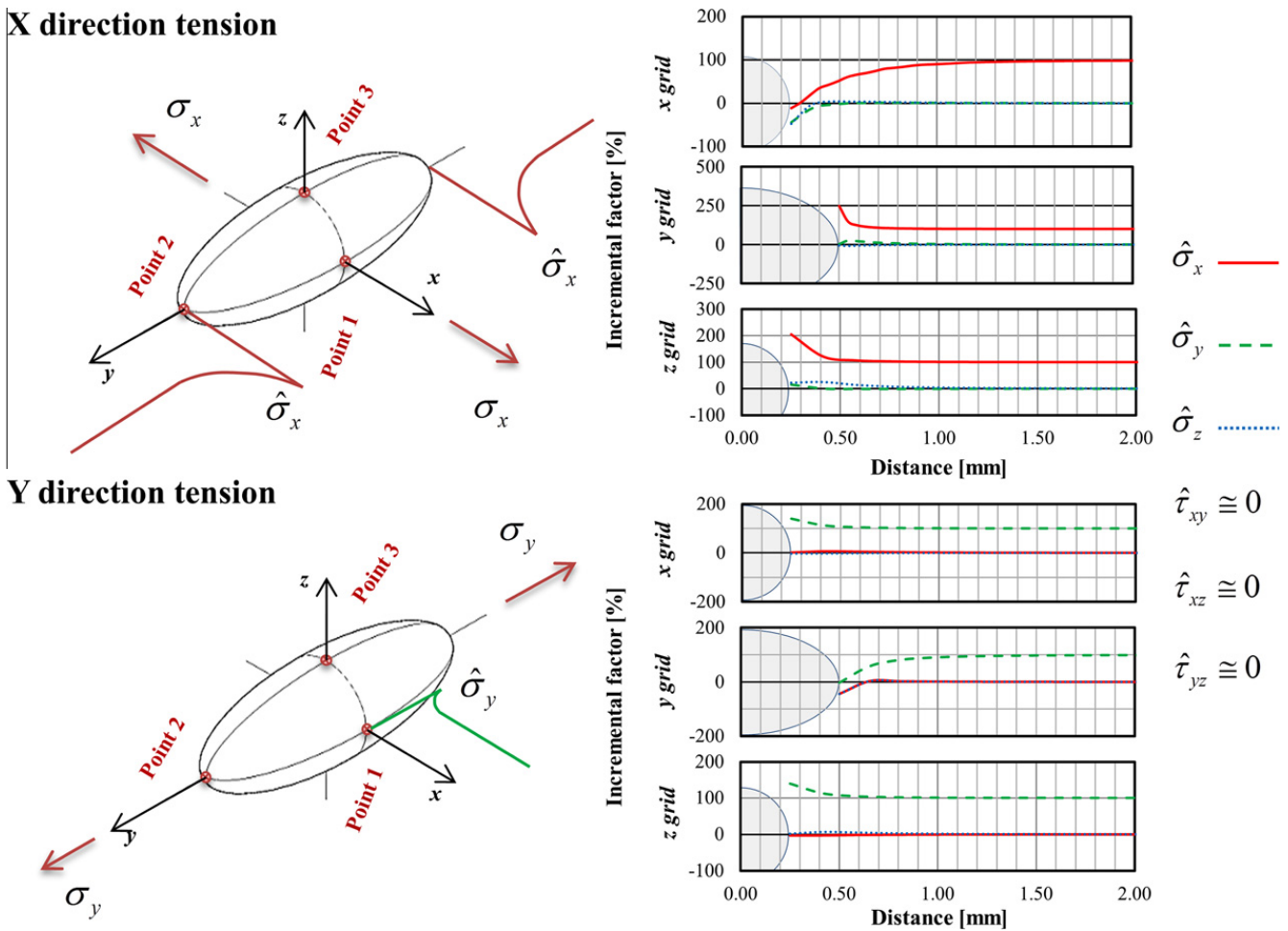


Fig. 5. Stress distribution around a prolate spheroid.

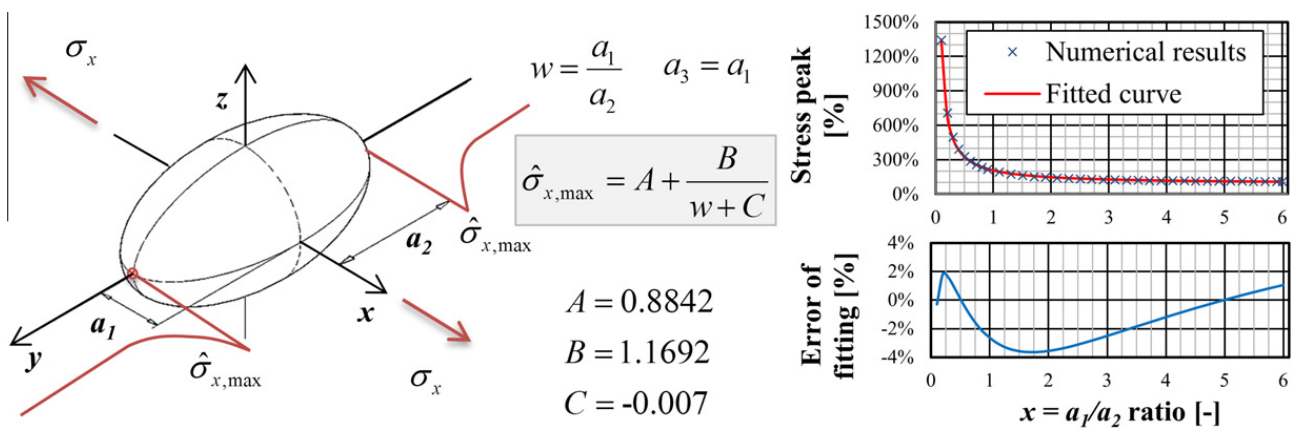


Fig. 6. Stress peak caused by the spheroid in the function of the radii ration.

In each case the homogeneous stress boundary was 100 MPa. We can see the comparison in Table 1 and the major stress-peak diagrams in Fig. 8.

Between the maximum of the major stress peaks – x direction tension σ_x (Point 2), and y direction tension σ_y (Point 1) – there is less than 2.21% difference. Where the stress should be zero (x direction tension σ_x at Point 1) the numerical solution converges to the analytical

value by increasing the finite element mesh density (Fig. 9).

Comparing the numerical and analytical solutions we observed a good match, therefore the analytical method could be used to calculate the stress field around a defect in a structural glass plate. The Eshelby method needs less computational time and has more accuracy than the numerical solution, so conclude that the Eshelby based

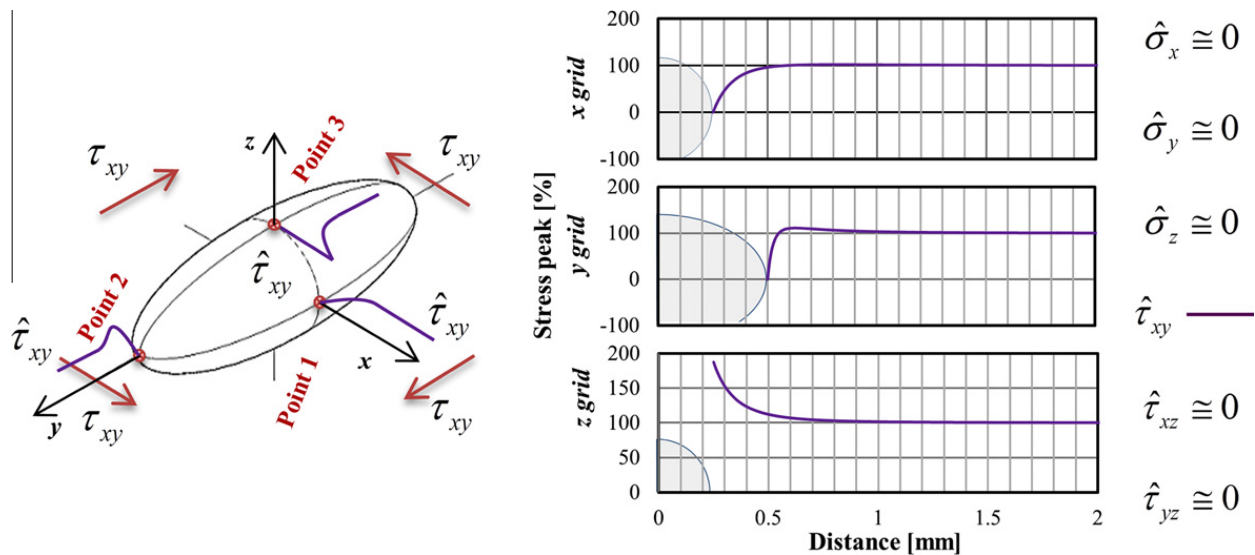


Fig. 7. Shear stress peak caused by the spheroidal inhomogeneity.

Table 1 Comparison of analytical and numerical results.

Load	Stress	Point 1		Point 2		Point 3	
		Analytical (MPa)	Numerical (MPa)	Analytical (MPa)	Numerical (MPa)	Analytical (MPa)	Numerical (MPa)
x Direction tension (100 MPa)	x	0.00	-1.49	238.32	243.71	244.09	244.94
	y	-49.35	-49.30	0.00	0.55	19.71	20.31
	z	-69.81	-68.34	-6.53	-5.88	0.00	0.33
y Direction tension (100 MPa)	x	0.00	0.15	-43.57	-44.76	-2.74	-2.70
	y	142.04	142.01	0.00	-1.02	142.04	142.13
	z	-2.74	-2.76	-43.57	-44.89	0.00	0.03
xy Direction shear (100 MPa)	xy	0.00	1.50	0.00	1.53	187.50	186.26

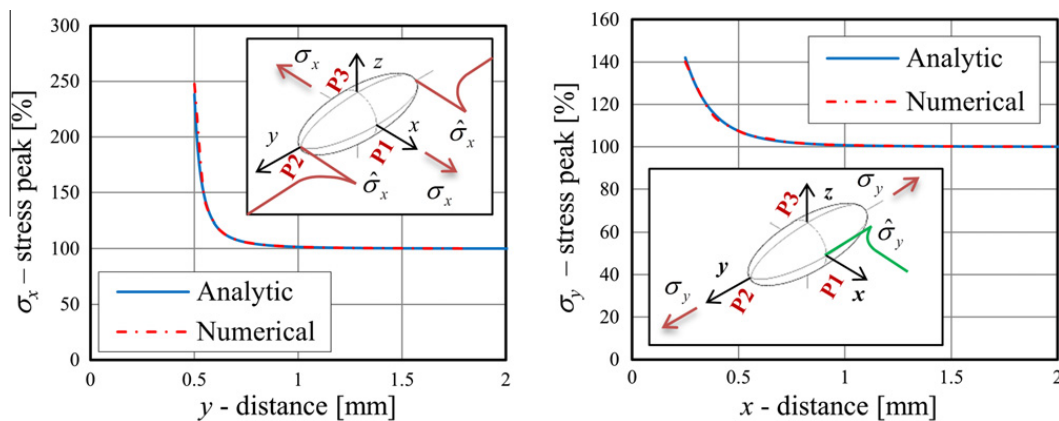


Fig. 8. Comparison of analytic and numerical solutions - major stress peaks (x direction tension - σ_x (y grid); y direction tension - σ_y (x grid)).

analytical solution should be used in the further statistical process.

3. Inhomogeneity distribution

As we mentioned in the introduction our goal was to calculate a parameter which takes into account mechanically the randomly formed (during the manu-

facturing process) inhomogeneities in the structural glass plate.

We have received the statistical information from a Hungarian float-glass manufacturing company (Guardian Hungary Co. Ltd). During the discussion we will only present the theoretical models and equations of the analysis, but the exact input parameters will be treated as proprietary. Only the results of the analysis will be quantified.

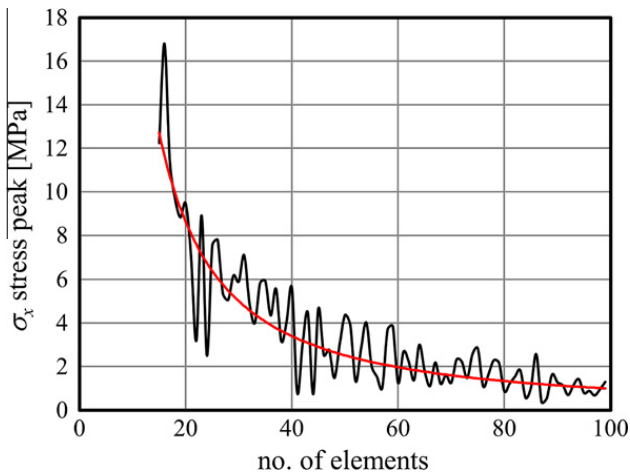


Fig. 9. σ_x at Point 1 in the function of the mesh density.

We have received the data stream of the position, the quantity and the type of all the optical defects. We used a Visual Basic script to evaluate the information and construct the necessary probability density functions. The optical size classification was not relevant to use in a mechanical analysis, so we have used optical microscopy to determine the radii ratio density function of the bubbles. We measured 63 specimens during the analysis. All the measured bubbles were optically allowed in an architectural glass.

We assumed that we have **four** probability density functions, **three** of the functions related to the *spatial position* of the inhomogeneity, and **one** is related to the *radii ratio* of the spheroids.

Fig. 10 shows the theoretical probability density functions of the defects.

We have approximated the functions in Fig. 10 as follows:

$$\begin{aligned}
 f_1(x) &= \frac{1}{l_x} \left[1 - \frac{\mu}{2} \cos\left(\frac{2\pi x}{l_x}\right) \right] \quad \text{if } -\frac{l_x}{2} \leq x \leq \frac{l_x}{2}, \\
 f_2(y) &= \frac{1}{l_y} \quad \text{if } -\frac{l_y}{2} \leq x \leq \frac{l_y}{2}, \\
 f_3(z) &= \sum_{i=1}^5 p_i \delta(z - z_i), \\
 f_4\left(w = \frac{a_1}{a_2}\right) &= \frac{\alpha k [(w - \gamma)/\beta]^{\alpha k - 1}}{\beta [1 + \{(w - \gamma)/\beta\}^\alpha]^{k+1}}.
 \end{aligned} \tag{1}$$

In $f_1(x)$ function μ is a disparity parameter, which shows the density difference between the middle and the outer region, l_x is the ribbon size. We assumed that $f_2(y)$ is uniform, where l_y is the trim size. The density values along the height was received in discrete form – in $f_3(z)$ p_i is the density values of each layer, δ is the Dirac function, z_i is the location of each layer. $f_4(w)$ was found to be a 4 point Dagum distribution; k , α , β are shape parameters, γ is a location parameter; the Anderson-Darling test statistic value was 0.22644. We have assumed that the random variables are **independent**.

The probability, that the worst defect is in the point of maximal stress – calculated with a homogeneous material – is approximately zero. The aim of the analysis is to find a **stress limit** ($\hat{\sigma}_{lim}$) in the glass plate – laden with defects – which will not be exceeded with a 95% probability. Therefore if we have 100 glass plates and we load them the same way – because of the defects the maximal stress peak is going to vary – but we count the 95 smallest maximal stress values in each plate, we can define a stress value (the largest of the 95) which is not going to exceeded with 95% probability, this is the limit we are searching for. Statistically we could describe as follows:

$$P(\sigma < \hat{\sigma}_{lim}) \leq 0,95 \iff F(\hat{\sigma}) = \int_{-\infty}^{\hat{\sigma}_{lim}} f(\hat{\sigma}) d\hat{\sigma} = 0,95 \tag{2}$$

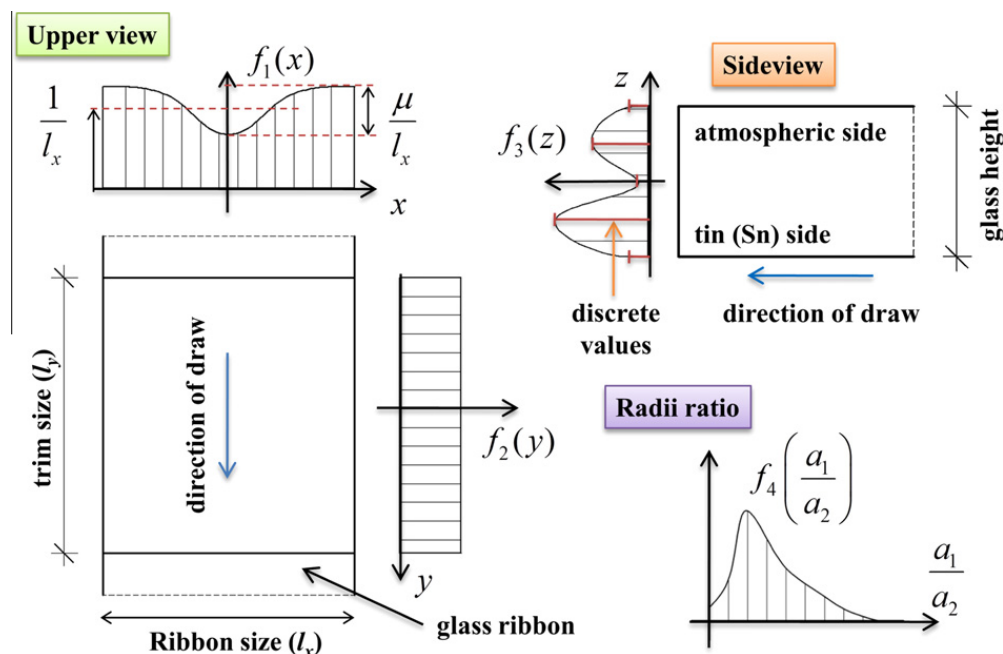


Fig. 10. Probability density functions of inhomogeneities.

where $\hat{\sigma}$ is the stress peak caused by the inhomogeneity; it could be calculated as $\hat{\sigma} = \sigma(x, y, z)\gamma_{ell}(w)$, where $\sigma(x, y, z)$ is the homogeneously (without defects) calculated stress-field, $\gamma_{ell}(w)$ is a stress increasing factor of the ellipsoidal inhomogeneity (function of the shape). $f(\hat{\sigma})$ is the probability density function of the stress peaks ($\hat{\sigma}$). $F(\hat{\sigma})$ is the cumulative distribution function of stress peaks ($\hat{\sigma}$). Integrating (2) we get the desired stress limit.

If we have the stress limit, we could divide it with the homogeneously calculated maximal stress value. We get a dimensionless coefficient, which could be used to multiply the initial (homogeneously calculated) maximal stress value to apply the effect of the inhomogeneities in glass.

$$\gamma_{lim} = \frac{\hat{\sigma}_{lim}}{\sigma_{max}} > 1, 0 \quad (3)$$

where σ_{max} is the homogeneously calculated maximal stress value, $\hat{\sigma}_{lim}$ is the stress limit, which will not be exceeded with a 95% probability and γ_{lim} is the dimensionless coefficient. This coefficient could be used to multiply the effect side in a design standard. Therefore we do not need to know the strength (resistance side) of the glass to take the mechanical effect of the voids into account because it appears only at the effect side as a load factoring coefficient.

To calculate (2) we have to transform the original random variables (1) to a new $\hat{\sigma}$ random variable. The transformation of these multiple random variables can only be carried out in special cases; therefore the statistical calculation was performed using numerical simulations in MATLAB.

3.1. Statistical simulation

Numerical analysis of the proposed model is carried out by using Monte Carlo simulation. The basic flow-chart of the computer code is presented in Fig. 11.

The simulation study is designed to answer the following questions:

- What is the mechanical effect of the inhomogeneities in a glass plate exposed to bending load?
- Does the size of the structural element statistically affect the stress peaks caused by defects?
- Which plate aspect ratio has the least increasing effect?

- Does the relationship of the drawing (manufacturing) direction and bending direction affect the possible stress peaks?
- How much difference we got if the tension side is the atmospheric side or the tin side of the float glass?

All numerical experiment setup was conducted in the following manner:

1. The code loads the input parameters, where l_x is the ribbon size, l_y is the trim size and h is the height of the manufactured glass plate; we used 4 mm thick jumbo size glass plates (3210 × 6000 mm). l_a and l_b is the actual side lengths of the structural element cut out from the original glass plate. pr is the ratio of $pr = l_b/l_a$. In the manufactured glass plate the average defect number in n and nu is the disparity parameter in $f_1(x)$ (14). sim_no is the number of simulations carried out on one type of glass plate. $load$ is a function, which tells us the homogenous plate's stress distribution in the function of the spatial coordinates; in present study we modelled the plate as a simply supported beam, so the load function was the following:

$$\sigma(y, z) = \left(\sigma_{max} - 4y^2 \frac{\sigma_{max}}{l_b^2} \right) z, \quad (4)$$

(4) tells us the axial stress in the direction of l_b , the other stress components were approximated by zero, σ_{max} is the homogeneously calculated maximal axial stress.

We have three switch parameters: The first is dir_bend ; this parameter tells us that the direction of bending is parallel ($dir_bend=1$) or perpendicular ($dir_bend=2$) to the drawing direction. If dir_bend is zero the direction of the loading is random with the probability of 50–50%.

The second switch parameter is dir_tens . With this parameter we could decide that the tin side ($dir_tens=1$) or the atmospheric side ($dir_tens=2$) will be the actual bottom side – in our case the tension side – of the structural element. If dir_tens is zero, we make the decision randomly (50–50%).

The third switch is loc_plate . This parameter is 1 or 2. If $loc_plate=1$, we cut the structural plane from the

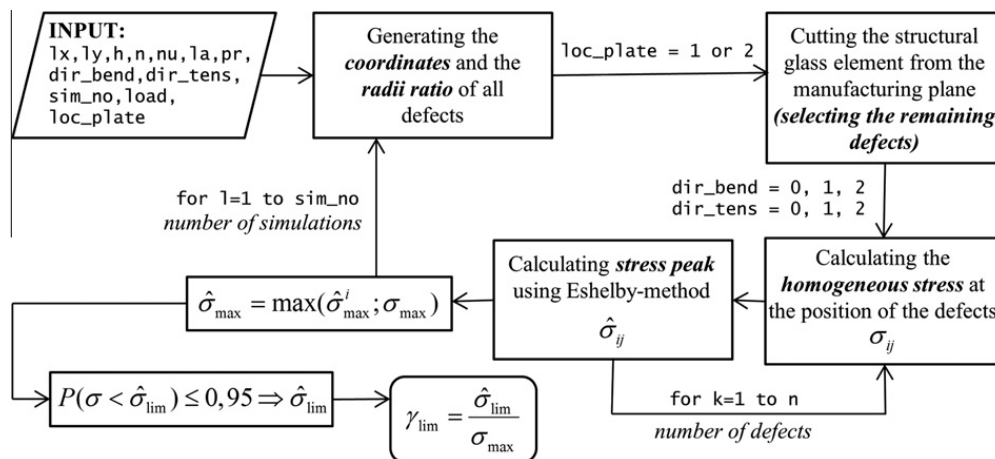


Fig. 11. Simplified scheme of numerical simulation.

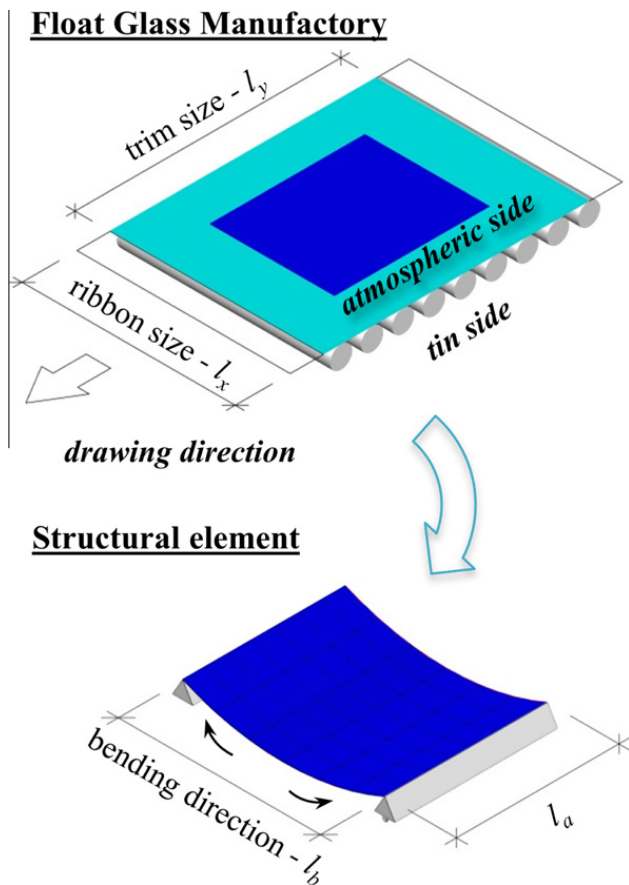


Fig. 12. Schematic figure of experimental setup.

middle of the ribbon, where we could find less defects; or if `loc_plate=2` we take the final plate from the outer region, where the density of the bubbles is higher.

2. The first step is to generate the defects in the glass plate to simulate a manufacturing process. The spatial coordinates and the radii ratios of the inhomogeneities are generated according to the probability density functions (14).
3. At this moment we have n defects in the plate $l_x \times l_y$. Now we cut the actual structural element from the

whole plate. The numerical aspect of this operation is that we choose only the defects which are present in the $l_a \times l_b$ area. (Fig. 12)

4. According to the switch parameters a subroutine calculates the homogeneous stress at the position of the defects. In this simulation the defects does not have any spatial extension, they are considered as points in the glass volume.
5. Another subroutine – made by Meng et al. (2011) – calculates the maximal stress peak around the ellipsoidal inhomogeneity. In this case the defect is placed in an infinite space and exposed by the homogeneous stress calculated before.
6. We take the maximum of the maximal stress peaks calculated at the previous step and the homogeneously calculated maximal stress value – $\hat{\sigma}_{\max} = \max(\hat{\sigma}_{\max}^i; \sigma_{\max})$.
7. We return to step 2 and carry out another experiment, until we reach the desired number.
8. After sorting $\hat{\sigma}_{\max}$, and taking the value which belongs to the 0.95 quantiles, we divide it by σ_{\max} , and we reach a factoring coefficient which could be used to multiply the original stress value to consider the mechanical effect of the inhomogeneities.

3.1.1. Convergence of simulation

Application of the Monte Carlo method requires an accurate analysis of the convergence process. To calculate a size-effect coefficient, we first had to evaluate the number of simulations that leads us to a sufficiently precise result. We could assume that increasing the number of experiments simulated on one type of specimen, the statistical value should converge to the actual factoring value. Convergence in the function of the number of simulations is shown in Fig. 13. Therefore, the value 50,000 is used for the number of simulations in the numerical analysis.

4. Results

The major aim of the simulation was to describe the mechanical effect of the inhomogeneities. The simulated probability density and cumulative probability distribution functions of $\gamma_{\lim} = \hat{\sigma}_{\max} / \sigma_{\max}$ values are presented in Fig. 14 and Fig. 15. We could recognise that the inhomogeneities do not have any stress increasing effect compared to the homogeneously calculated maximal stress value with a 15.5% probability. It means that all inhomogeneity falls into the mid-plane, into the compressed or less tensioned regions and does not cause higher stress than the homogeneously calculated about 15.5% of time. The functions in Fig. 14 and Fig. 15 are typical examples for the factoring value distributions, not specified results of the analysis.

The factoring coefficient is always greater-than or equal to 1.00, because in step 6 it is calculated by dividing the maximal stress by the homogenous maximal stress value. If the inhomogeneities are not at the position of σ_{\max} , and they do not cause greater stress peak than σ_{\max} , the factoring coefficient shall be 1.00. That is the reason why a great density peak could be recognised in the histogram (Fig. 14) at value 1.00.

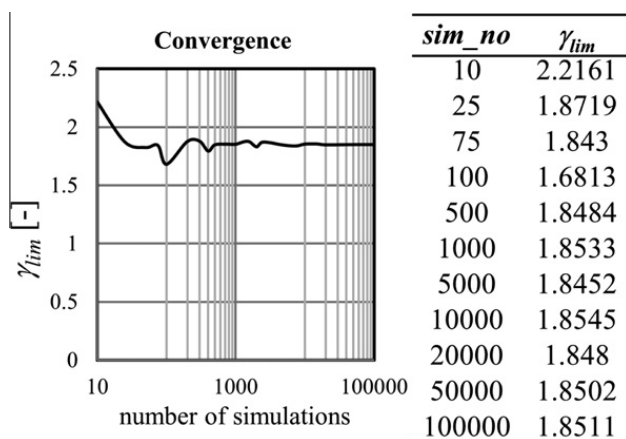


Fig. 13. Convergence in the function of the number of simulations.

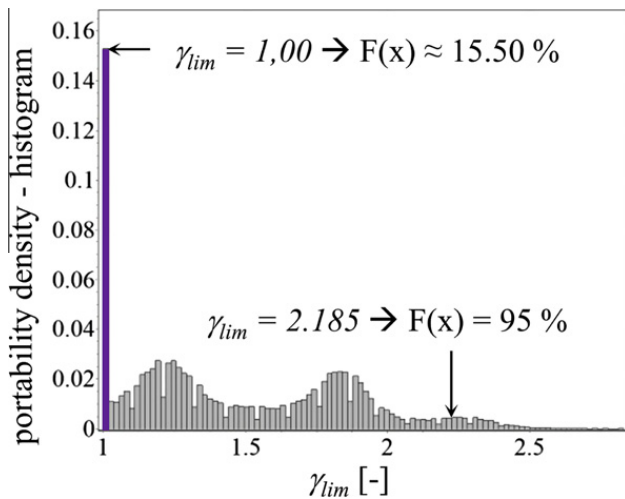


Fig. 14. Probability density of factoring values.

4.1. Does plate ratio affect the factoring coefficient?

After the definition of γ_{lim} we could investigate the size effect of the glass plates. As mentioned in the introduction we worked with 4 mm thick glass. Therefore we changed only the plate's ichnographical size. Fig. 16 shows the factoring coefficient in the function of the plate's area. We could recognise that the effect of the defect increases by increasing the plate's size. As larger the plate the probability is higher having a sharp inclusion at a worse location. The minimal size of the glass was 0.4 m², and the largest size was 6.0 m².

In Fig. 17 we could recognise that the plate ratio has no noticeable effect on the factoring coefficient. Therefore we performed experiments aimed at confirming this negligible plate ratio effect. We left the plates size on 3.00 m², modifying the plate's ratio, we showed that the parameter has only a slight effect on the stress peak caused by defects. But it is negligible ($\approx 2\%$ in the range of $0.5 \leq l_b/l_a \leq 2.0$) compared to the size's effect. Therefore we could state that the γ_{lim} factoring coefficient is a size effect coefficient.

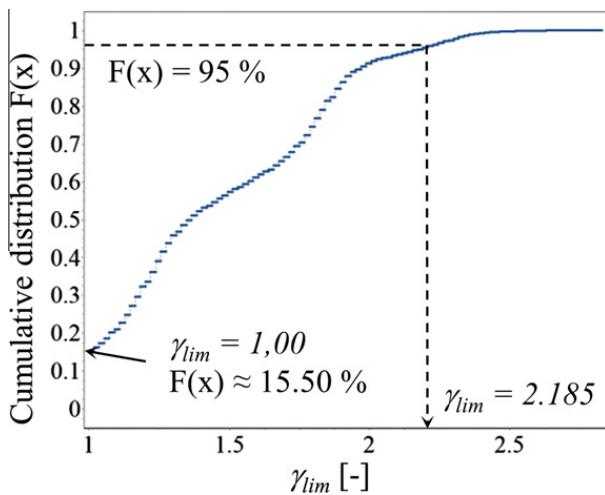


Fig. 15. Cumulative distribution functions of factoring values.

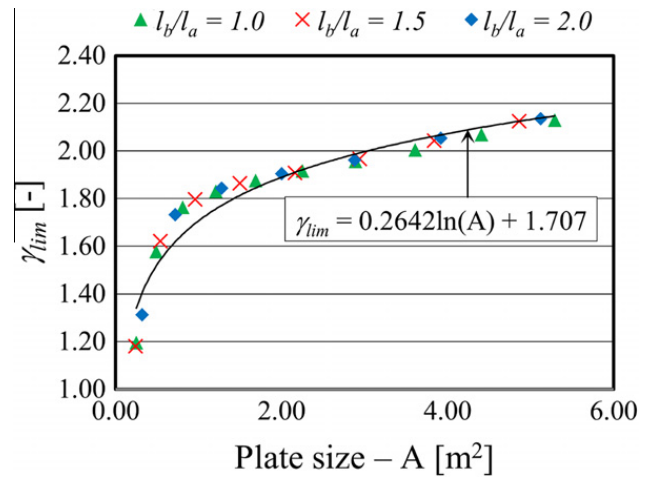


Fig. 16. Factoring coefficient (γ_{lim}) in the function of the plate's size.

4.2. Correlation between the bending and the drawing direction

Our goal was to help designers and factories, how to minimise the mechanical effect of the remaining inhomogeneities in structural glass elements using simple guidelines, for example to connect the bending with the drawing direction, or the tension side with the tin or the atmospheric side.

During current analysis we considered glass plates with the plate ratio of 1.5, $dir_tens=0$, $loc_plate=1$. We changed dir_bend from 0 to 2.

In Fig. 18 we could recognise that the relationship between the drawing and the bending direction (Fig. 12) is obvious. In every case if we take parallel the two directions we could decrease the effect of the defects.

The reason of the phenomenon is simple. Due to the drawing process the sphere shape bubble transforms into a spheroid with the larger radius parallel to the floating direction. Therefore if we consider a prolate spheroidal inhomogeneity loaded in the direction of the major principal axis (a_2) – in the direction of drawing (y) (Fig. 10) – (therefore the radii ratio is larger than 1.00 (Fig. 6)), the stress peak caused by the defect would be significantly

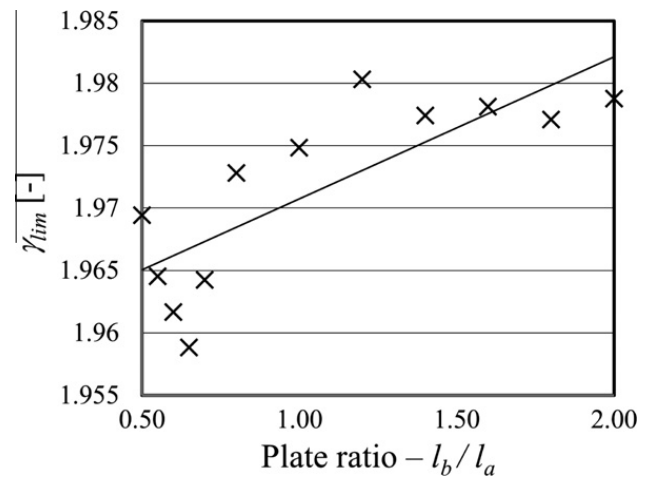


Fig. 17. γ_{lim} in the function of plate ratio (l_b/l_a).

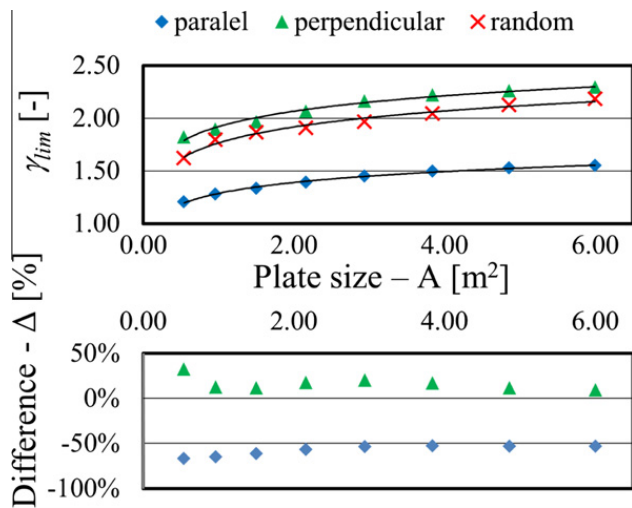


Fig. 18. γ_{lim} in the function of bending direction.

smaller than if we stress the defect perpendicular. Hence we construct the glass plate bent parallel to the direction of the drawing, the effect of the inhomogeneities going to be average 57.79% smaller than if we do not deal with this question and make the decision at random, and 63.62% smaller compared to the perpendicular way. The difference was calculated as follows:

$$\Delta = (\gamma_{lim,1} - \gamma_{lim,2}) / (\gamma_{lim,2} - 1), \quad (5)$$

where $\gamma_{lim,1}$ is the factoring coefficient compared to $\gamma_{lim,2}$.

4.3. Tin and tension side orientation

The inhomogeneity distribution along the thickness of the glass plate is not uniform, therefore we investigated, which orientation of the tension side is better for a unidirectionally bent glass plate. In Fig. 19 the factoring coefficient is presented in the function of the tin side orientation.

The diagram shows that if we use only the atmospheric side as the tension side, we could reduce the effect of the defects by 15.61% compared if we make the decision ran-

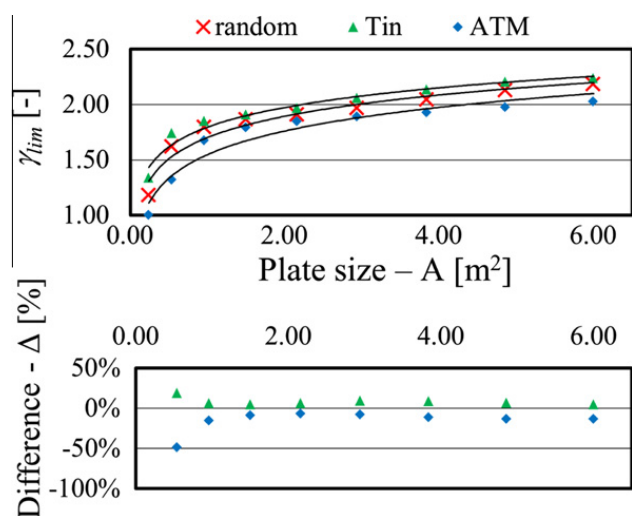


Fig. 19. γ_{lim} in the function of tension side orientation.

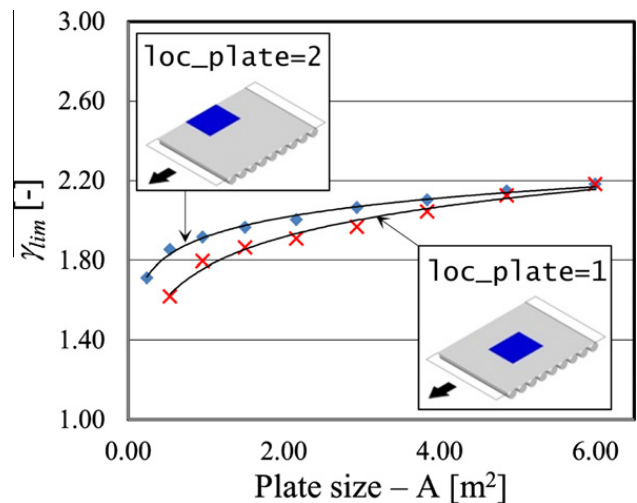


Fig. 20. γ_{lim} in the function of the original position.

domly. The reason for this phenomenon is that the defect density is higher near to the tin than the atmospheric side of the float glass ribbon. In Fig. 19 the difference was calculated in the same way as (5).

4.4. Original position on the ribbon

Because of the density differences of the defects along the ribbon, the original position of the structural element on the manufactured plate is relevant. The two possibilities are presented Fig. 20.

Fig. 20 shows that smaller plates extracted from the outer region had larger γ_{lim} , than the plates from the middle of the ribbon. However increasing the plate size the factoring coefficients are getting closer and closer to each other. Therefore we could conclude that plates from the middle region have statistically less defects, as a result: less stress increment. To take advantage of this phenomenon we should chose the more efficient structural elements from the middle, and the less ones from the outer region.

5. Conclusion and future plans

We worked out a method to calculate the effect of the glassy inhomogeneities (which take the largest part of the defects in float glass) remaining in glass after the manufacturing procedure. The defined coefficient shows the stress limit which will not be exceeded with a 95% probability. We found that the statistical effect of the defects is increasing by increasing the plate's size, therefore the calculated coefficient expresses a **size effect**.

Using this indicator factor we analysed designing concepts, and we proposed guidelines to decrease the mechanical effect of the voids. These suggestions are the following:

- The plate ratio has no major effect on the factoring coefficient.
- Using parallel bending direction as the drawing direction could reduce the effect by 57.79%.

- Using the atmospheric side as tension side reduces the effect by 15.61% compared to random decision.
- Planning the cutting layout in the function of the efficiency of the structural element could lead to optimal design.

Further plans include calculation factoring coefficient with complex stress fields as two directional bending, tempering or pin loading.

Acknowledgements

We are very grateful for specimens and the statistical database to Guardian Hungary Co. Ltd. and Chunfang Meng PhD for the evaluation of Eshelby solution. The micro-CT images were made by Csaba Dobó-Nagy PhD, we are grateful for his help.

This work is connected to the scientific program of the “Development of quality-oriented and harmonized R+D+I strategy and functional model at BME” project. This project is supported by the New Hungary Development Plan (Project ID: TÁMOP-4.2.1/B-09/1/KMR-2010-0002).

Appendix Analytical. Eshelby's solution

In the next section we would like to summarise the main theoretical steps Eshelby's analytical solution, which was used to compute the stress field around the elliptical void.

Eshelby (1957) pointed out that the stress disturbance in an applied stress-field due to the presence of an inhomogeneity can be simulated by an eigenstress caused by an inclusion when the eigenstrain¹ is chosen properly.

During the investigation we will confine ourselves to ellipsoidal shape inhomogeneities. We could define the Ω subdomain in a Cartesian coordinate system as follows (Fig. 21):

$$\frac{x^2}{a_1^2} + \frac{y^2}{a_2^2} + \frac{z^2}{a_3^2} \leq 1, \quad (\text{A.1})$$

where a_1, a_2, a_3 are the principal half axes of the ellipsoid. For static loading and isotropic materials we could define the Green function (Mura, 1987, p. 22). At this point we could divide the solution into two parts. There are different approaches for the *interior* points and the *exterior* points.

Interior. points

Owing to the work Eshelby, we know that the strain and the stress are constant inside in an ellipsoidal inclusion², so we can extract ε_{ij}^* and we could write the strain correlation as

¹ Eigenstress is a generic name given to self-equilibrated internal stress caused by one or several of eigenstrains in bodies which are free from any other external force and surface constraint. The eigenstress field are created by the incompatibility of eigenstrains. Eshelby (1957) referred to eigenstrains as a stress-free transformation strains. Example: non-elastic strains, thermal expansion, phase transformation, initial strains (Mura, 1987, p. 1).

² An inclusion has the same elastic moduli as the material (matrix), and it contains eigenstrains. (Mura, 1987, p. 177).

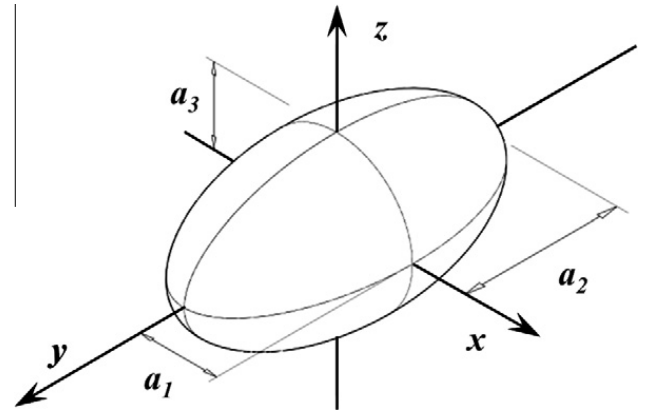


Fig. 21. Representation of an ellipsoidal shape inhomogeneity in Cartesian coordinate system.

$$\varepsilon_{ij} = S_{ijkl} \varepsilon_{ij}^* \quad \text{for } x \in \Omega, \quad (\text{A.2})$$

where S_{ijkl} is called the Eshelby's tensor (Mura, 1987, p. 77), ε_{ij}^* is the eigenstrains and ε_{ij} is the total strains. Originally the components of S_{ijkl} contains first and second term elliptic integrals, but we know from the microscopic investigation that the bubbles and the stones have a spheroid shape, thus the Eshelby's tensor could be simplified (Mura, 1987, p. 77):

$$\begin{aligned} S_{ijkl} &= S_{klij} = S_{ijkl}, \\ S_{1111} &= \frac{3}{8\pi(1-\nu)} a_1^2 I_{11} + \frac{1-2\nu}{8\pi(1-\nu)} I_1, \\ S_{1122} &= \frac{3}{8\pi(1-\nu)} a_2^2 I_{12} + \frac{1-2\nu}{8\pi(1-\nu)} I_1, \\ S_{1133} &= \frac{3}{8\pi(1-\nu)} a_3^2 I_{13} + \frac{1-2\nu}{8\pi(1-\nu)} I_1, \\ S_{1212} &= \frac{a_1^2 + a_2^2}{16\pi(1-\nu)} I_{12} + \frac{1-2\nu}{16\pi(1-\nu)} (I_1 + I_2). \end{aligned} \quad (\text{A.3})$$

All other non-zero components are obtained from the systematic permutation of 1, 2, 3 in a_i, I_i and I_{ij} . The components which cannot be obtained by cyclic permutation are equal to zero ($S_{1112} = S_{1223} = S_{1232} = 0$). In equation (A.3) ν is the Poisson's ratio. For a general ellipsoidal inclusion I_i and I_{ij} integrals are given by (Routh, 1895) and could be found in (Mura, 1987, p. 77).

Exterior. points

For an exterior point we could write (A.2) as

$$\varepsilon_{ij}(x) = D_{ijkl}(x) \varepsilon_{kl}^*, \quad (\text{A.4})$$

where D_{ijkl} gives us the effect of the eigenstrains in an arbitrary point x . (since ε_{ij}^* is constant). Ferrers (1877) and Dyson (1981) expressed that the integrals of (A.3) could be modified, therefore we simply change the lower integral limits to λ , where λ is the largest positive root of

$$\frac{x^2}{a_1^2 + \lambda} + \frac{y^2}{a_2^2 + \lambda} + \frac{z^2}{a_3^2 + \lambda} \leq 1, \quad (\text{A.5})$$

for $x \in D - \Omega$ and zero for $x \in \Omega$. After a few modifications we could express D_{ijkl} . (Mura, 1987, p. 85).

The final result holds for both interior and exterior points, with the fact that if $x \in \Omega$ then $\lambda = 0$, in this case all derivatives of I_i and I_{ij} vanish, and we can determine an expression for D_{ijkl} becomes S_{ijkl} which is equal to the original Eshelby's tensor (A.3). (Mura, 1987, p. 88)

Equivalent. inclusion method

So far we have only a solution for the original Eshelby's problem, but we have to find a solution for the mechanical effects of voids and rigid inhomogeneities³ in the material. So our problem could be described as a subdomain Ω (inhomogeneity) with different elastic moduli (C_{ijkl}^*) in the infinite D domain (matrix). Our goal is to describe the stress disturbance caused by the presence of an ellipsoidal inhomogeneity in the material.

To calculate the effect of the inhomogeneity we will define an equalling arbitrary eigenstrain, which could be used in the original Eshelby's solution to describe the stress field caused by the inhomogeneity.

First we have to calculate the fictional eigenstrain, which describes the effect of the inhomogeneity. We will start with the initial condition, that in the inclusion (subdomain Ω) the stress has to be equal in the original problem and in the fictional, Eshelby's problem.

$$\begin{aligned} \sigma_{ij}^\infty + \sigma_{ij} &= C_{ijkl}^*(\varepsilon_{kl}^\infty + \varepsilon_{kl}), \\ \text{sigma}_{ij}^\infty + \sigma_{ij} &= C_{ijkl}^*(\varepsilon_{kl}^\infty + \varepsilon_{kl} - \varepsilon_{kl}^{ast}), \end{aligned} \tag{A.6}$$

where σ_{ij}^∞ is the stress, ε_{ij}^∞ is the strain in infinity, σ_{ij} is the additional stress ε_{ij} is the additional strain peak, ε_{ij}^* is the fictional eigenstrain. The two cases should be equal, so we could write

$$C_{ijkl}^*(\varepsilon_{kl}^\infty + \varepsilon_{kl}) = C_{ijkl}(\varepsilon_{kl}^\infty + \varepsilon_{kl} - \varepsilon_{kl}^*). \tag{A.7}$$

From the Eshelby's solution we know, that

$$\varepsilon_{ij} = S_{ijkl}\varepsilon_{kl}^*. \tag{A.8}$$

Eq. (A.7) could be written as

$$C_{ijkl}^*(\varepsilon_{kl}^\infty + S_{klmn}\varepsilon_{mn}^*) = C_{ijkl}(\varepsilon_{kl}^\infty + S_{klmn}\varepsilon_{mn}^* - \varepsilon_{kl}^*). \tag{A.9}$$

From equation (A.9) the fictional eigenstrain ε_{ij}^* could be determined.

However in glass construction we have a common problem with nickel sulphide (NiS) defects (nickel sulphide has a different thermal expansion coefficient, so during the tempering procedure it may cause unexpected failure), so sometimes our inhomogeneity has its own eigenstrains. (A.7) changes as

$$C_{ijkl}^*(\varepsilon_{kl}^\infty + \varepsilon_{kl} - \varepsilon_{kl}^p) = C_{ijkl}(\varepsilon_{kl}^\infty + \varepsilon_{kl} - \varepsilon_{kl}^p - \varepsilon_{kl}^*), \tag{A.10}$$

where ε_{kl}^p is the true eigenstrain of the inhomogeneous inclusion. Eq. (A.8) changes to

$$\varepsilon_{ij} = S_{ijkl}(\varepsilon_{kl}^* + \varepsilon_{kl}^p) = S_{ijkl}\varepsilon_{kl}^{**}. \tag{A.11}$$

In this case to calculate the necessary eigenstrain ε_{ij}^{**} we could use

$$C_{ijkl}^*(\varepsilon_{kl}^\infty + S_{klmn}\varepsilon_{mn}^{**} - \varepsilon_{kl}^p) = C_{ijkl}(\varepsilon_{kl}^\infty + S_{klmn}\varepsilon_{mn}^{**} - \varepsilon_{kl}^{**}). \tag{A.12}$$

To calculate the strain and the stress peak values, we could use the original Eq. (A.6) with the addition of the remote stress and strain.

$$\begin{aligned} \hat{\varepsilon}_{ij} &= \varepsilon_{ij}^\infty + S_{ijkl}\varepsilon_{kl}^{**}, \\ \hat{\sigma}_{ij} &= \sigma_{ij}^\infty + C_{ijkl}(S_{klmn}\varepsilon_{mn}^{**} - \varepsilon_{kl}^{**})\text{in}\Omega, \\ \hat{\varepsilon}_{ij}(x) &= \varepsilon_{ij}^\infty + D_{ijkl}(x)\varepsilon_{kl}^{**}, \\ \hat{\sigma}_{ij} &= \sigma_{ij}^\infty + C_{ijkl}D_{klmn}(x)\varepsilon_{mn}^{**}\text{for } x \in D - \Omega. \end{aligned} \tag{A.13}$$

All eigenstrains are stress-free so we have to subtract the effect from the total strain when we calculating the stresses in the inclusion. There are no eigenstrains in the exterior part, so it has no effect on it.

References

Bartuška, M., et al., 2001. Glass Defects Glass Service, Inc.
 Benedetti, A., Geotti-Bianchini, F., Fagherazzi, G., Riello, P., Albertini, G., De Riu, L., 1994. SAXS study of the micro-inhomogeneity of industrial soda lime silica glass. *Journal of Non-Crystalline Solids* 167, 263–271.
 Dyson, F.D., 1981. The potentials of ellipsoids of variable densities. *Quarterly Journal of Pure and Applied Mathematics* 25, 259–288.
 Eshelby, J.D., 1957. The determination of the elastic field of an ellipsoidal inclusion, and related problems. *Proceedings of the Royal Society of London Series A. Mathematical and Physical Sciences* 241, 376–396.
 Eshelby, J.D., 1959. The elastic field outside an ellipsoidal inclusion. *Proceedings of the Royal Society of London Series A. Mathematical and Physical Sciences* 252, 561–569.
 Eshelby, J.D., 1961. Elastic inclusion and inhomogeneities. *Progress in Solid Mechanics* 2, 89–140.
 Ferrers, N.M., 1877. On the potentials of ellipsoids, ellipsoidal shells, elliptic laminae and elliptic rings of variable densities. *Quarterly Journal of Pure and Applied Mathematics* 14, 1–22.
 Jin, Y., Wang, Z., Zhu, L., Yang, J., 2011. Research on in-line glass defect inspection technology based on Dual CCFL. *Procedia Engineering* 15, 1797–1801. <http://dx.doi.org/10.1016/j.proeng.2011.08.334>.
 Liu, H.G., Chen, Y.P., Peng, X.Q., Xie, J.M., 2011. A classification method of glass defect based on multiresolution and information fusion. *International Journal of Advanced Manufacturing Technology* 56, 1079–1090, 10.007/s00170-011-3248-z.
 Meng, C., Heltsley, W., Pollard, D.D., 2011. Evaluation of the Eshelby solution for the ellipsoidal inclusion and heterogeneity. *Computers and Geosciences*. <http://dx.doi.org/10.1016/j.cageo.2011.07.008>.
 Molnár, G., Molnár, L.M., Bojtár, I., 2012. Mechanical classification of structural glass. *Materials Engineering-Materialove Inzinerstvo* 19 (2), 71–81.
 Mura, T., 1987. *Micromechanics of Defects in Solids: Mechanics of Elastic and Inelastic Solids*. Kluwer Academic.
 Peng, X., Chen, Y., Liu, H., Xie, J., Gu, C., 2011. An online defect classification method for float glass fabrication. *Glass Technology – European Journal of Glass Science and Technology Part A* 52 (5), 154–160.
 Peng, X., Chen, Y., Yu, W., Zhou, Z., Sun, G., 2008. An online defects inspection method for float glass fabrication based on machine vision. *International Journal of Advanced Manufacturing Technology* 39, 1180–1189. <http://dx.doi.org/10.1007/s00170-007-1302-7>.
 Routh, E.J., 1895. Theorems on the attraction of ellipsoids for certain laws of force other than the inverse square. *Philosophical Transactions of the Royal Society of London Series A* 186, 897–950.

³ When the elastic moduli of an ellipsoidal subdomain of a material differ from those of the remainder (matrix), the subdomain is called an *ellipsoidal inhomogeneity*. Example: voids, cracks, precipitates. (Mura, 1987, p. 177).